Physica Scripta

PAPER

Analysis of ternary $AlGaX_2$(X = As, Sb) compounds for opto-electronic and renewable energy devices using density functional theory

Physica Scripta

PAPER

Analysis of ternary $AlGaX_2$(X = As, Sb) compounds for opto-electronic and renewable energy devices using density functional theory

RECEIVED
23 April 2021

REVISED
13 August 2021

ACCEPTED FOR PUBLICATION
23 August 2021

PUBLISHED
6 September 2021

M Waqas Iqbal[1], **Mazia Asghar**[1], **N A Noor**[1], **Hamid Ullah**[1], **Tausif Zahid**[2], **Sikandir Aftab**[3] and **Asif Mahmood**[4]

[1] Department of Physics, RIPHAH International University, Campus Lahore, Pakistan
[2] Department of Electrical Engineering, RIPHAH International University, Campus Lahore, Pakistan
[3] Electrical Engineering department, Simon Fraser University, Burnaby, Canada
[4] College of Engineering, Chemical Engineering Department, King Saud University Riyadh, Saudi Arabia

E-mail: naveedcssp@gmail.com

Keywords: Ab-initio investigations, R-3m space group of $AlGaX_2$, Direct bandgap materials, optical properties, figure of merit

Abstract

Based on the First-principles calculations, we have investigated the opto-electronic properties of $AlGaX_2$(X = As, Sb). We find that the $AlGaX_2$(X = As, Sb) is energetically stable due to lower formation enthalpy. Additionally, the dynamical stability is also confirmed by phonon calculation and found no-imaginary frequencies in the phonon-spectra. Interestingly, both $AlGaAs_2$ and $AlGaSb_2$ compounds possesses semiconductor nature with a direct bandgap of 1.40 eV and 0.70 eV, respectively. For the technological applications of $AlGaX_2$(X = As, Sb), we have analyzed optical properties in terms of absorption of photon energy and polarization. A strong absorption peaks are observed in the visible region. Moreover, the thermoelectric properties are calculated in terms of electrical/thermal conductivities, Seebeck coefficient, and figure of merit (ZT). Thermal parameters are critical for determining a material' thermal stability across the wide range of temperatures. We expect that our calculated properties of $AlGaAs_2$ and $AlGaSb_2$ compounds could pave a new route for the applications in the optoelectronics and thermoelectric devices.

1. Introduction

Ternary semiconductors are utilized in a number of applications such as non-linear optics, opto-electronics, electro-optics, particularly in photovoltaic solar cell materials and many other thermoelectric devices at room temperature [1–3]. Therefore, these semiconducting materials are largely being studied all over the world for their suitability of being used in a variety of projects. The antimony chalcogenides and bismuth based solid solutions have been found to be high- efficiency devices for being utilized in countless thermoelectric applications [4, 5]. For being used in such applications, the candidate materials must have low thermal conductivity, high Seebeck coefficient and high electrical conductivity. In chalcogenides, Bi_2Se_3 [6, 7] semiconductor has been explored for thermoelectric applications. Scientists of the current era are very much interested in finding ternary semiconductors for the area of photoelectric technology [8] and thermoelectric technology [9], because they have good thermoelectric features, low effective mass, direct band gap and higher optical absorption coefficient [10, 11].

Environmentally friendly way of power production is very important thing that is possible by harvesting waste refrigeration and heat through thermoelectric technology and solid state cooling. This enables invertible conversion between electricity and thermal energy [12, 13]. The conversion efficiency of a candidate compounds in terms of its thermoelectric (TE) technology is computed through its figure of merit (ZT). ZT is dimensionless parameter and is given as $ZT = \frac{S^2\sigma T}{(\kappa_e + k_L)}$, where k_L is lattice thermal conductivity, κ_e is electric conductivity, T represents working temperature, σ symbolizes lattice constant and S stands for Seebeck coefficient. There are

two basic requirements for getting a high figure of merit one is high power factor and second is the low thermal conductivity [14–17]. Recently, Mg-based ternary semiconducting materials at room temperature have deeply been investigated [18, 19]. The structure of MgSrX (X = Si, Sb, Bi) are better thermoelectric compounds [20, 21].

A part of Pnictides family type III–III–V_2 compounds that are crystallized in tetragonal space group is represented by Ternary $AlGaAs_2$ semiconductors [22]. In addition, some sorts of ordered structures in III-V ternary semiconducting materials such as CuPt [23, 24], chalcopyrite [25, 26] and CuAu [27, 28] kinds have also been investigated. DFT being a valuable standard tool for the evaluation of mechanical and electronic properties is widely used by the scientists. The related literature have been observed while using first-principle methods for the analysis of the physical features of the ternary semiconductors that is quite in line with the results obtained through experimental studies [29–32].

To our knowledge, there is no other report available in the existing literature. The pure $AlGaAs_2$ and $AlGaSb_2$ compounds with $R\bar{3}m$ space group have not yet been investigated in terms of their physical properties. We have studied the thermoelectric and opto-electronic response of $AlGaAs_2$ and $AlGaSb_2$. Our calculated results exhibit energetically and dynamical stable nature of the material due its lower formation enthalpy and no imaginary frequencies in the phonon spectra. We find that both the materials possess a direct bandgap semiconducting nature. Moreover, the calculated optical parameters and ZT values show that these materials could be promising in the field of opto-electronic and thermoelectric.

2. Computational method

We employed Wien2k code to investigate structural and opto-electronic properties that based on full-potential linearized augmented plane wave (FP-LAPW+lo) method [33]. All finding of properties are density functional theory (DFT) based calculations, where the PBEsol generalized gradient approximation (GGA) [34] is used to calculate the structural parameters. In addition, for the calculations of accurate opto-electronic properties, we employed modified Becke and Johnson (mBJ) potentials [35]. The reason for choosing mBJ potential is that it gives accurate prediction of bandgap according to experimental calculated values of bandgap [36, 37]. Further, for the prediction of more accurate value of bandgap very close to experimental values, we also used spin–orbit coupling (SOC) for the calculation of opto-electronic properties [38, 39]. Corrections to the modified Becke-Johnson (mBJ) potential measurements have been made for spin–orbit coupling (SOC) to demonstrate the effect of spin–orbit coupling (SOC) on the values of band difference, state density and thermal properties of both the current ternary semiconductors.

The convergence of the plane wave basis set is reached at the minimum cutoff energy i.e. $R_{MT} \times K_{max} = 8.0$, where R_{MT} is the smallest muffin tin radius, and K_{max} is embodied as the peak value for the cutoff wave vector [40]. Using the Monkhorst-Pack system [41], the Brillion zone sampling technique was carried out for the k-space aggregation of 1000 points in the entire Brillion zone. The R_{MT} muffin tin radius values were chosen as 2.21 atomic units (au), 2.34 au, 2.34 au and 2.5 au respectively for Al, Ga, As and Sb atoms during all calculations. Inside the muffin tin spheres, the wave function was extended to $l_{max} = 10$ [42] and the charge density expansion was cut at $G_{max} = 16\ (a.u)^{-1}$ [43]. The convergence rate per formula unit of the absolute charge density difference between the consecutive loops was less than $0.0001|e|$, where the self-consistent calculations were presumed to converge [44].

For the calculations of electronic transport properties,we have used BoltzTrap code [45]. The phonon spectra are calculated using Phonopy [46] code with VASP [47] as calculator. The temperature (K) and chemical potential (μ) analysis of electrical and thermal conductivities, Seebeck co-efficient and figure of merit are investigated that based on the Boltzmann equation's semi-classical treatment by incorporating approximations like that of the time of relaxation and the rigid part [47].

3. Results and discussion

3.1. Structural parameters and their stability

We used the relaxed structure of ternary $AlGaX_2$ (X = As, Sb) compounds with space group of $R\bar{3}m$ (no. 166) to explored structural, opto-electronic and transport properties. The unit cell of $R\bar{3}m$ with trigonal symmetry is presented in figure 1. In this unit cell of $AlGaX_2$, the positions of Al, Ga and As/Sb are 3a, 3b and 6c respectively according to Wyckoff positions. In the method of volume optimization, plots of energy verses volume of both compounds are achieved while using PBEsol-GGA [34]. Consequently, the lattice constant (a_0, c_0) and bulk modulus (B_0) of studied compounds are examined using the Murnaghan equation [48] and their calculated values are listing in Table 1. Form the Table 1, we have noted that calculated values of lattice parameters (a_0, c_0) for both compounds using PBEsol-GGA are good comparable to other theoretical reported values [49]. From

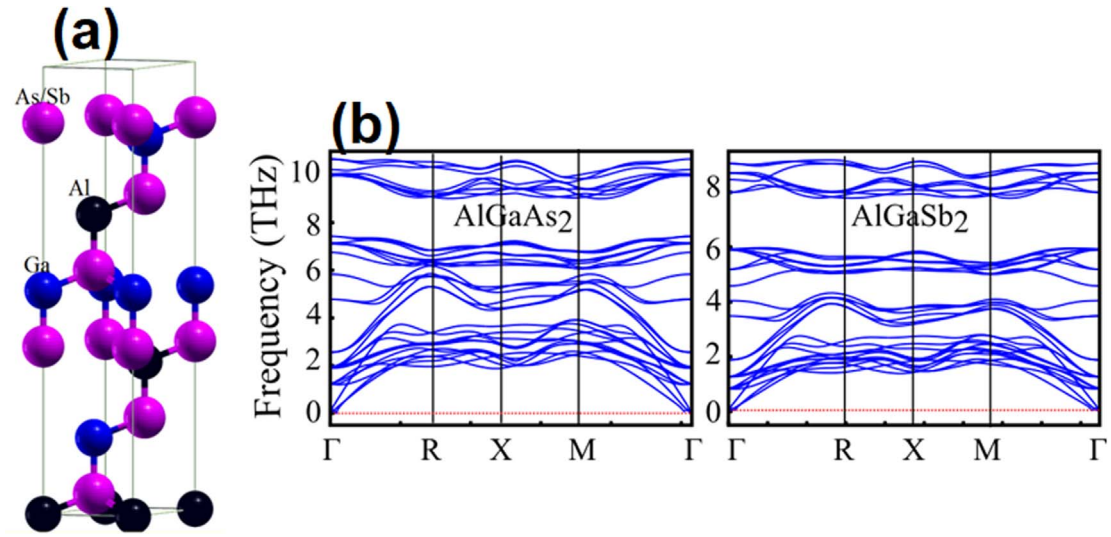

Figure 1. (a) Crystal structure of $AlGaX_2$ (X = As, Sb) in $R\bar{3}m$ space group. Here black, blue, and pink balls represent the Al, Ga, and As/Sb atoms, respectively (b) the phonon spectra of $AlGaX_2$ (X = As, Sb).

Table 1. The lattice constant a_o(Å) and c_o(Å), bulk modulus B_o(GPa), Enthalpy of formation ΔH_f (eV), for$AlGaX_2$ (X = As, Sb)compared and calculated with existing data.

Parameters	$AlGaAs_2$		$AlGaSb_2$	
	PBEsol-GGA	Other	PBEsol-GGA	Other
a_o	4.02	4.06[a]	4.36	4.40[a]
c_o	19.83	19.87[a]	21.50	21.55[a]
B_o	40.82		33.05	
ΔH_f	−0.188	−0.146[a]	−0.472	−0.412[a]

[a] [49].

literature, we noted that both compounds are not explored experimentally. So, in order to confirm their stability in $R\bar{3}m$ (no. 166) space group, we calculate phonon dispersion spectra of studied compounds (see figure 1b).

Our calculated plots of phonon dispersion spectra show that no happening of negative frequency in considered Brillouin zone. Therefore, it indicates that studied compounds are thermodynamically stable. Further, thermodynamically stability also investigates by measuring formation enthalpy (ΔH_f). We used the following expression for the estimation of ΔH_f:[50]

$$\Delta H_f = E_{total}(Al_l Ga_m X_n) - lE_{Al} - mE_{Ga} - nE_X \quad (1)$$

The right side includes the overall energies of substances and their energies in this equation, respectively, of component parts. Here, l, m, and n are the numbers of atoms within the composites. We found that for all compounds studied, ΔH_f represents negative values and verified their reliability at this point.

3.2. Opto-electronic properties

For any material, DFT based calculation of electronic properties are highly dependent on its electronic structure. By utilizing this fact, band structures (BS) and density of states (DOS) plots of both compounds ($AlGaAs_2$ and $AlGaSb_2$) are used to manipulate their electronic properties. For calculations of BS as well as DOS plots, a novel computational approach named mBJ-LDA potential equipped with SOC has been successfully employed in order to avoid the underestimation of band gaps. From figure 2, it is obvious that both compounds ($AlGaAs_2$ and $AlGaSb_2$) reveal direct band gap nature having values of 1.40 eV and 0.7 eV, respectively. It can be observed from Table 2 that the calculations executed by PBEsol + SOC package led to the underestimation of calculated bandgap and this observation is in line with the previously calculated PBE-GGA functional results [51]. For an inclusive analysis of electronic dimensions and the band energy existence of materials, electronic density of state (DOS) is very significant [52]. Our calculated DOS results for both $AlGaAs_2$ and $AlGaSb_2$ reveals the occurrence direct bandgaps by virtue of conduction band minimum corresponding to Al-3p and valence band maximum

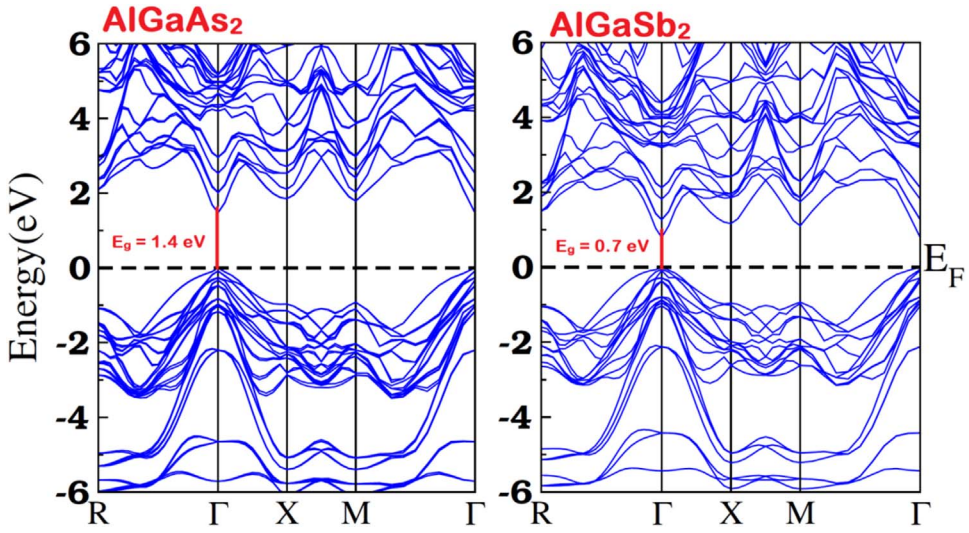

Figure 2. The calculated band structures using mBJ + SOC potentials for $AlGaX_2$ (X = As, Sb).

Table 2. The calculated E_g(eV): direct bandgap using mBJ + SOC potential and optical parameters at 0 energy for $AlGaX_2$ (X = As, Sb).

	E_g(eV)	$\varepsilon_1(0)$	n(0)	R(0)
$AlGaAs_2$	1.40	8.69	2.94	0.24
$AlGaSb_2$	0.7	11.17	3.34	0.29

mainly consisting of Ga-4p and As-4p states. Therefore, this study allows us to take advantage of investigated materials for high performance optoelectronic devices. Note that to our knowledge there is not enough experimental and theoretical literature available in this trigonal phase $R\bar{3}m$. We have compared our calculated bandgap of $AlGaAs_2$ compound with the available Tetragonal ($p\bar{4}m2$) with band gap 0.99 eV [53] and body centered tetragonal ($I\bar{4}2d$) phase with a gap of 0.86 eV [53]. Interestingly, our calculated band gap is significantly higher (1.40 eV) for $AlGaAs_2$ and no literature available for comparison of $AlGaSb_2$.

The semiconductor nature and the inter band transitions are the key factors deciding the feasibility of a material towards optoelectronic applications [54]. To probe the optical features of the ternary semiconductors ($AlGaX_2$ (X = As, Sb)), their complex dielectric constants were calculated given by the relation [55]; $\varepsilon(\omega) = \varepsilon_1(\omega) + i\varepsilon_2(\omega)$, Here, $\varepsilon_1(\omega)$ and $\varepsilon_2(\omega)$ denote the real and imaginary parts of complex dielectric constant, respectively, as depicted in figure 4(a). The calculation of both real and imaginary parts provides insights and perspectives for extinction, refraction and reactivity of a material. By employing photon energies in the range of 0–12eV, various important dielectric parameters including refraction n(ω), absorption $\alpha(\omega)$, extinction k(ω), reflectivity R(ω) and optical conductivity $\sigma(\omega)$ were calculated as represented in figures 4(b) and 5(a)−(c). By substituting Sb with As (i.e. changing ternary composition from $AlGaAs_2$ to $AlGaSb_2$) the high intensity peak is displaced from 13.21 eV to 16.27 eV thus revealing the shifting of $\varepsilon_1(\omega)$ spectra towards lower energy region by said substitution. We also noted from the calculated value of $\varepsilon_1(\omega)$, at low energy polarization/dispersion is increased because electron cloud of Sb ions is lower than that of As ions. Moreover, the static dielectric constants $\varepsilon_1(0)$ for both compounds have been derived from $\varepsilon_1(\omega)$ versus energy plots showing complete concurrence with Penn's rule $\varepsilon_1(0) \approx 1 + (\hbar\omega_p/E_g)^2$. In this equation, $\hbar$ represent the Planck's constant and ω_p is the plasma frequency [56] and the resultant values are shown in tabular form in Table 1.

On behalf of permitted electronic transitions of the compounds $AlGaX_2$ (X = As, Sb), the calculated $\varepsilon_2(\omega)$ values are presented in figure 4(a). As the energy gap values of $AlGaAs_2$ and $AlGaSb_2$ are 1.4 eV and 0.70 eV, respectively thus $\varepsilon_2(\omega)$ remain zero for all photons having energy less than that of respective energy gaps. While, figure 3(a) illustrates that the electronic transitions corresponding to unoccupied 3p (Al) states and the 3p(As)/4p(Sb) states, yields threshold of imaginary part $\varepsilon_{12}(\omega)$. Thus, figure 3(a) is a clear-cut evidence that the investigated ternary ($AlGaX_2$ (X = As, Sb)) exhibit a perfect photon absorption tendency in visible as well as infra-red (IR) region of electromagnetic (EM) spectrum.

Furthermore, the absolute value of $\varepsilon_1(\omega)$ and the refractive index n(ω) are related by a relationship of $n_0^2 = \varepsilon_1(0)$. As seen in figure 4 (a), a direct transfer from occupied states to unoccupied states could be

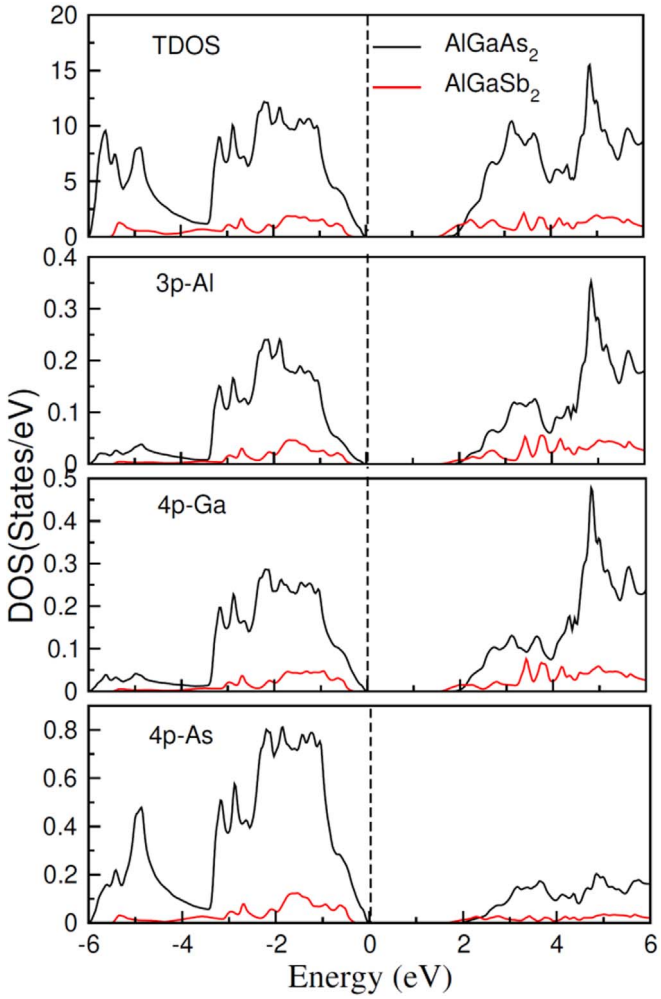

Figure 3. Calculated density of states (DOS) using mBJ + SOC potentials for $AlGaX_2$ (X = As, Sb).

demonstrated via $\varepsilon_2(\omega)$. The real portion of the refractive index n(ω) specifies the visibility of the materials when the received photon drops on the surface of the sample and is described as [57]. The value of n(ω) relies on the light's wavelength as well as the light is scattered into its basic colours. Although the imaginary component is described by the following formula, i.e., the extinction coefficient k(ω) [58]. The value of k(ω) larger than zero represents the capacity of the material to absorb photons. It is noted from the graphs as shown in figure 4(b) that the peaks both for n(ω) and k(ω) lie in the reduced energy area, which is gradually reduced by increasing more energy. The dynamic characteristics is shown by the n(ω) peaks in the infrared region [59] of it and also represent 2.94 value at n(0) as shown in table 2.

Likewise, a dielectric constant can also be used to achieve the absorption coefficient $\alpha(\omega)$ [60]. The intensity of light when moving through the material can be provided by $\alpha(\omega)$. Low energy absorption is primarily due to transitions, as seen in figure 5(a), across tightly packed energy sources. Moreover, for the energy spectrum of $AlGaSb_2$ and $AlGaAs_2$ respectively, maximal peaks occur from 3.6 eV to 8.0 eV as is seen in the absorption map with a set of related peaks after this energy absorption value declines gradually. The optical conductivity of materials $\sigma(\omega)$ depends strongly on the imaginary dielectric function portion [61]. In the $\sigma(\omega)$ plot, multiple peaks are shown as seen in figure 5(b), which is related to the transfer of electrons. For $AlGaSb_2$, its value is maximal since it has a low band gap value at intermediate energies, optical conductivity is very high, demonstrating the transitions between closely-spaced energy bands. The stability of the surface, atomic levels and positions is clarified by investigating the reflectivity [61]. As seen in figure 5(c), in the reflectivity spectrum, it is greater at minimum absorption. Minimum energy loss and maximum absorption in the low energy region of electromagnetic radiation make these materials acceptable to IR and visible applications.

3.3. Electronic transport properties

Another effective means of satisfying global energy needs is the conversion of heat into electrical energy. Therefore, analysis of electronic transport properties plays a vital role in the field of energy needs. One of the

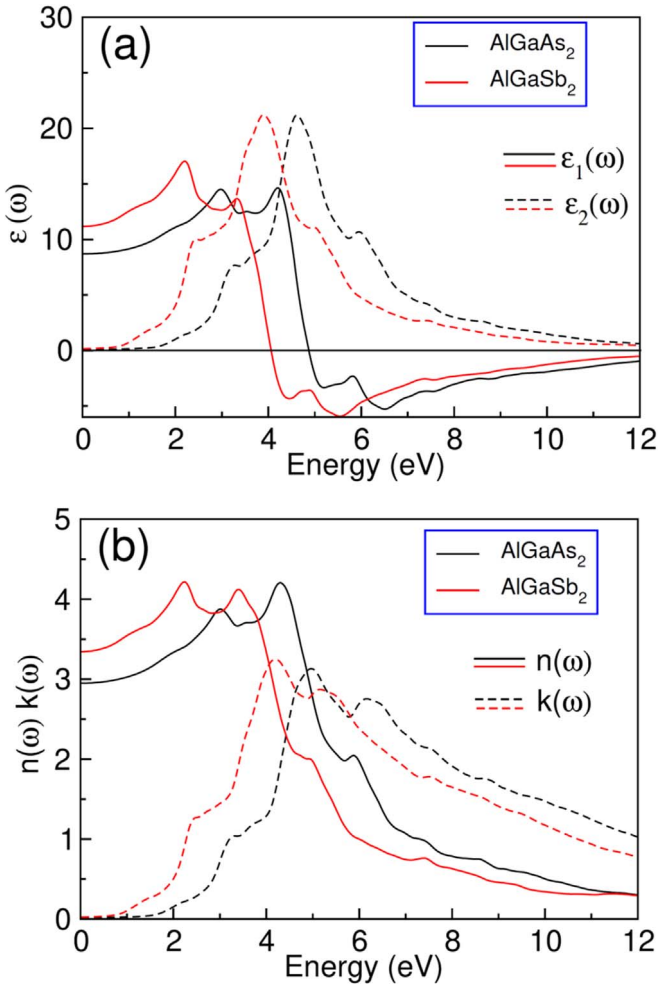

Figure 4. The inferred (a) real part $\varepsilon_1(\omega)$, imaginary part $\varepsilon_2(\omega)$, (b) refractive index n(ω), (d) the extinction co-efficient k(ω) using mBJ + SOC potential for $AlGaX_2$ (X = As, Sb).

significant constituents of chalcopyrite structures have applications in solar cell and electronic transport systems based on ternary compounds. We have evaluated the electronic transport properties of $AlGaX_2$ (X = As, Sb), as presented in figures 6(a)–(f) and figures 7(a)–(d) with chemical potential (μ) and temperature (K). The following expressions given in [62, 63] are used to determine thermoelectric properties using BoltzTrap software. For calculating the thermoelectric efficiency, we used the expression: $ZT = \frac{S^2\sigma T}{(\kappa)}$, to evaluate the performance of ternary semiconductors. Here, S represents the Seebeck coefficient in above expression, σ is stand for electrical conductivity, κ is electronic thermal conductivity of ternary structures and T is temperature in Kelvin. By improving σ and S, but reducing κ, the volume can be increased. In all calculations of transport properties, relaxation time (τ) also play important role and used to assist thermal and electrical conductivity, as demonstrated by the classical Boltzmann transport principle. Here, for our calculations τ is kept constant because of BoltzTraP code.

Electrical conductivity (σ/τ) is the operational of thermoelectric instruments and the quantity of carrier movement, while chemical potential (μ) is the volume of energy necessary for the transporter to travel toward coulomb repulsion. We calculate σ/τ of ternary $AlGaX_2$ (X = As, Sb) compounds against μ and temperature (K) depicted in figures 6(a) and (b) respectively. Figure 6(a) show the σ/τ against μ plot, where positive (negative) values of chemical potential are connected top-type (n-type) features of materials. We noted that maximum value of σ/τ in n-type side is 2.62×10^{20} $1/\Omega$ms of σ/τ at -1.45 eV for $AlGaAs_2$. The electron concentration at the edge of the valence band is smaller in the conduction band relative to the hole transporters. There is also an improvement for $AlGaAs_2$ in σ/τ from $0.06 \times 10^{18}/\Omega$ms to $1.16 \times 10^{18}/\Omega$ms at a temperature range of 200–600K. Contrary, with the rise from $0.16 \times 10^{18}/\Omega$ms to $1.4 \times 10^{18}/\Omega$ms, the linearly boost in σ/τ up to 600K is noted for $AlGaSb_2$. Calculated results of $AlGaX_2$ (X = As, Sb) showed that relative to $AlGaSb_2$, the $AlGaAs_2$ compound has less electrical conductivity.

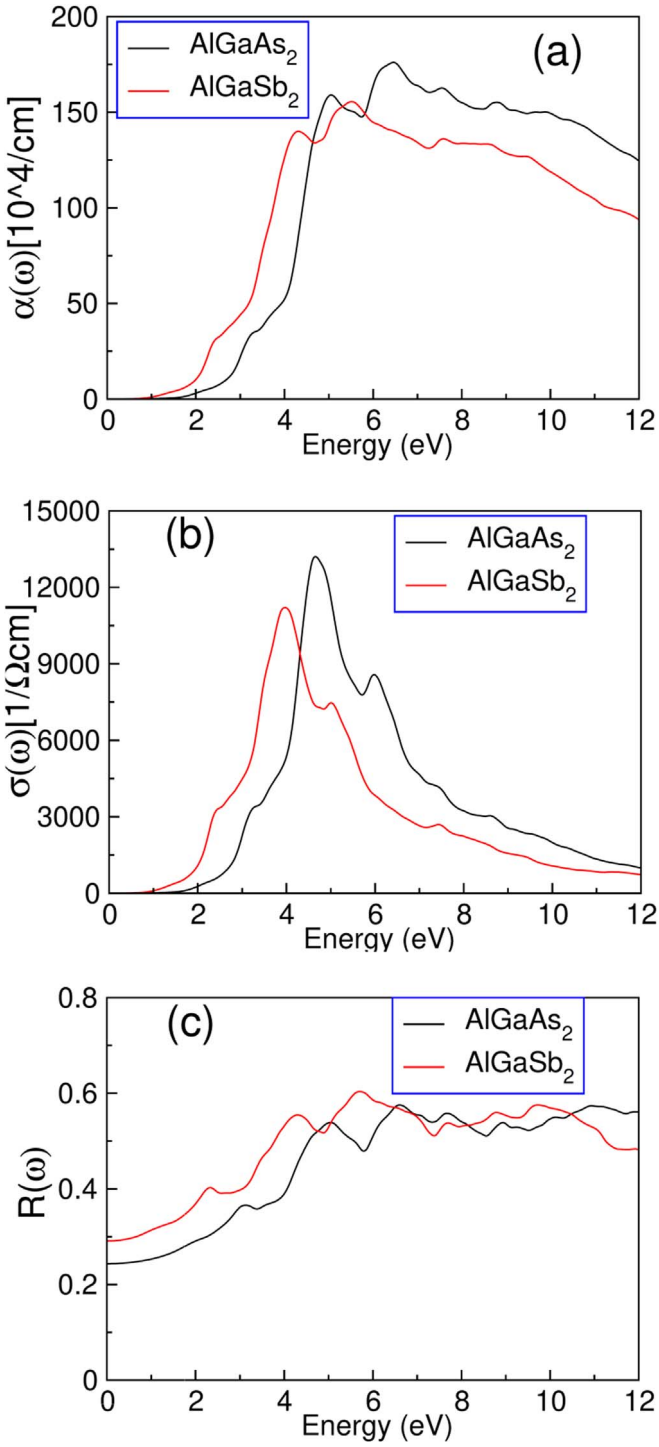

Figure 5. The inferred (a) absorption coefficient $\alpha(\omega)$, (b) optical conductivity $\sigma(\omega)$, (c) reflectivity $R(\omega)$ using mBJ + SOC potential for $AlGaX_2$ (X = As, Sb).

Thermal conductivity (κ) that based from the contribution of electronic (κ_e) part and lattice vibrations (κ_l) part in all solids [64] and actually are involved in the process of heat transfer. In our calculations of κ, we ignored the lattice vibrations (κ_l) part because of very low κ values in ternary semiconductors [65, 66]. Figure 6(c) reflects the values of electronic thermal conductivity (κ_e/τ) versus chemical potential, while figure 6(d) indicates the values of κ_e/τ versus temperature. If seen from figure 6(c) for metallic-like frameworks because of small contribution of phonons, identical response of κ_e/τ is noted as σ/τ. A variance in temperature reaction from electrical conductivity is identified in κ_e/τ. For $AlGaAs_2$ and $AlGaSb_2$, the measured values of κ_e/τ at room temperature are 0.09×10^{14} (W (mKS)$^{-1}$) and 0.10×10^{14}(W (mKS)$^{-1}$) respectively, and the temperature rise, its values of κ_e/τ is also rise.

In terms of power factor ($\sigma S^2/\tau$) calculations, $AlGaAs_2$ is more desirable than $AlGaSb_2$; however, the latter compound can undergo improved transport of phonons as heavyweight atoms act as a phonon rattler to inhibit

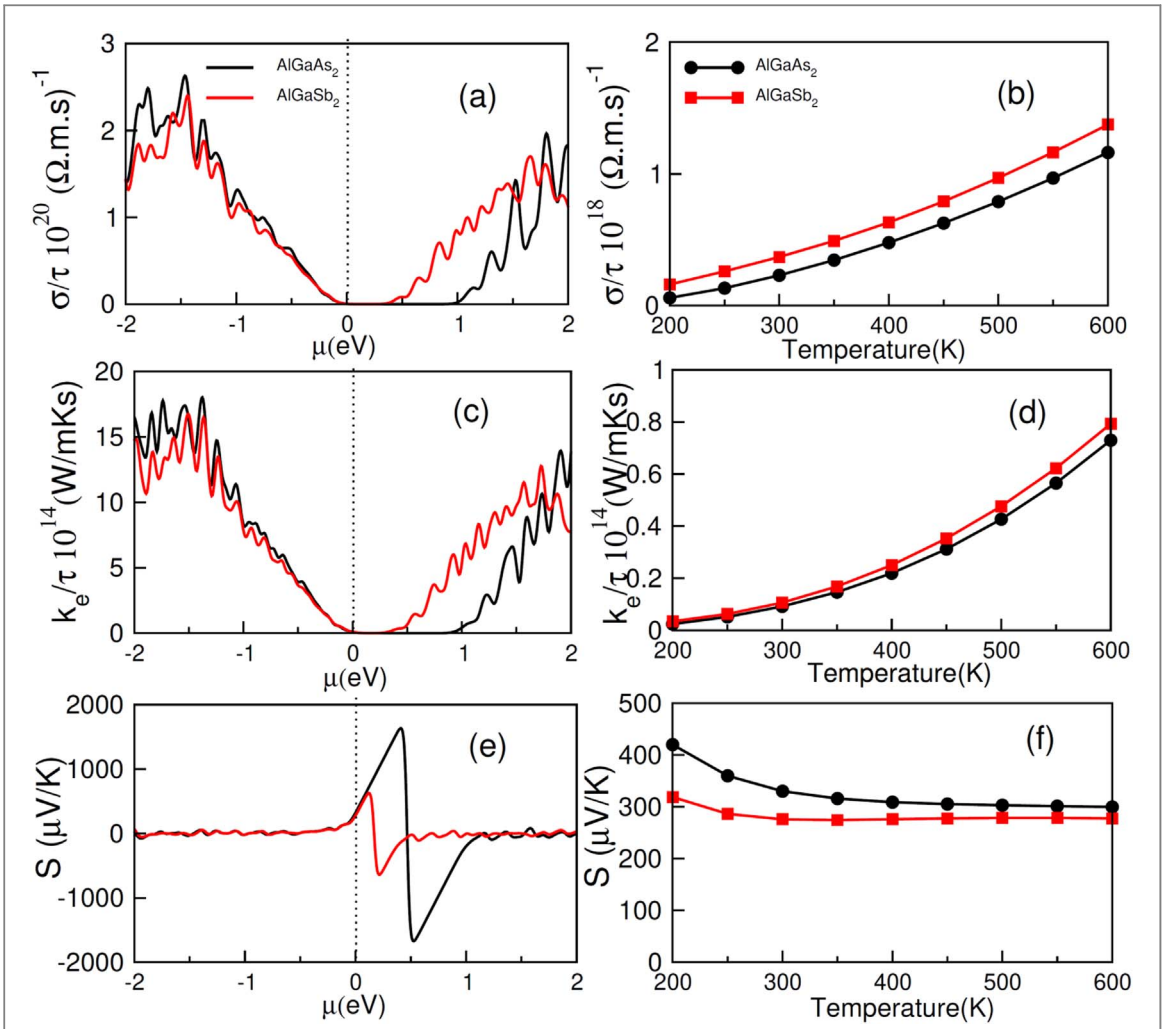

Figure 6. The calculated electrical (σ/τ), thermal (k_e/τ) conductivities and Seebeck coefficients (S) for $AlGaX_2$ (X = As, Sb) using mBJ + SOC potential.

thermal conductivity of lattice. Figure 6(e) and 6(f) reflect Seebeck co-efficient (S) as a function of μ and T. Figure 6(e) considered $AlGaAs_2$ to have maximum values of μ than $AlGaSb_2$. In comparison, $AlGaAs_2$ has high values of 0.42 eV at 1650 μV K^{-1} and 0.5 eV at 1700 μV K^{-1}, respectively. Electrons are thus, dominant. Therefore, for $AlGaSb_2$ 0.12 eV (555 μV K^{-1}) and −0.22 eV (700 μV K^{-1}), holes and electron withdraw each effects in order to stabilize those that decrease S.

The element $\sigma S^2/\tau$ measures a material's power in thermoelectric systems. Illustration of figure 7 (a) and 7(b) reflects the values of power factor versus μ and respectively of power factor versus temperature. $AlGaAs_2$ has a higher S, which is why it's value of $\sigma S^2/\tau$ is high. Within −1 to −2.0 eV for n-type and after 0.5 eV for p-type, peaks of $\sigma S^2/\tau$ occur for both ternary semiconductors. In $AlGaAs_2$, higher σ/τ and S improved their $\sigma S^2/\tau$ than in $AlGaSb_2$. Figures 7(c), (d) shows a value of figure of merit (ZT) to develop for the analysis of thermoelectric efficiency. The ZT values are high at about 1 for n and p-type conductions in $AlGaAs_2$. Figure 7(d) indicates a small rise in ZT versus temperature reaction. With increasing temperature (300K to 600K), the value of ZT also linearly increases. Overall, $AlGaAs_2$ is high ZT value at room temperature that is 0.82 as compared to $AlGaSb_2$ because its ZT value is 0.79. Comparatively, $AlGaAs_2$'s high ZT values make it a more suitable candidate for thermoelectric than $AlGaSb_2$.

4. Conclusion

In this paper, chalcopyrite $AlGaX_2$ (X = As, Sb) with $R\bar{3}m$ space group explored theoretically with the help of DFT. Our calculation of the negative values of formation enthalpy and phonon band dispersions having no negative frequency shows that studied structures are kinetically stable. Further, structural parameters, which indicates, in accordance with existing results, an increase in the lattice parameter a_0(Å) on the transfer from arsenide to antimony atoms. For transport and optoelectronic assets, we have used the modified Becke-Johnson

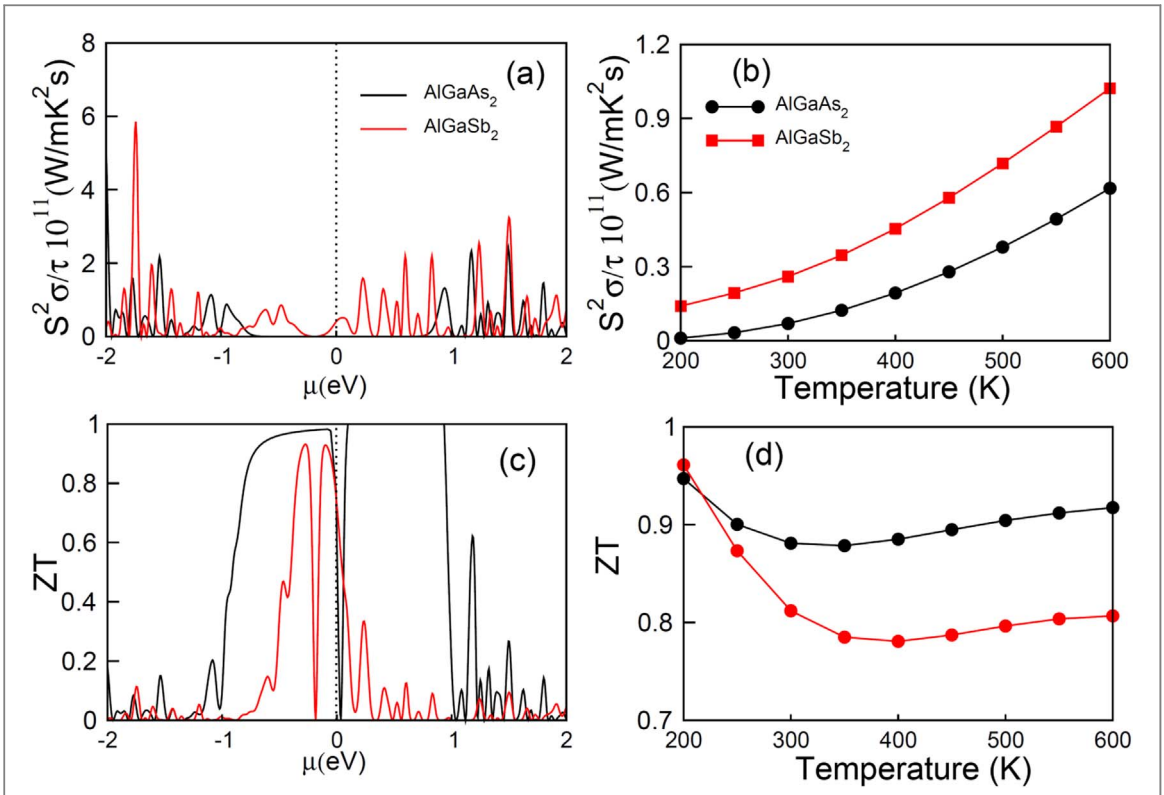

Figure 7. The calculated power factors ($S^2\sigma/\tau$) and figure of merit (ZT) for $AlGaX_2$ (X = As, Sb) using mBJ + SOC potential.

(mBJ) plus spin–orbit coupling (SOC) functional potential to resolve the functional PBEsol-GGA underestimation of the band gap. Our findings say that the electronic band difference is decreased from 1.40 eV to 0.68 eV when moving from $AlGaAs_2$ to $AlGaSb_2$. The exact energies obtained from the absorption coefficient and extinction coefficient for $AlGaAs_2$ and $AlGaSb_2$ show its better operate in visible to IR region for the applications of optoelectronic devices. More importantly, the high ZT value at room temperature of 0.82 and 0.79 (unity as a function of μ) indicates that the $AlGaAs_2$ and $AlGaSb_2$ tested are feasible from the point of view of thermoelectric application. The measured findings offer a wider understanding of their use in optoelectronic and energy mining applications.

Acknowledgments

The authors would like to acknowledge Researcher's Supporting Project Number (RSP-2021/43), King Saud University, Riyadh, Saudi Arabia.

Data availability statement

The data that support the findings of this study are available upon reasonable request from the authors.

ORCID iDs

N A Noor https://orcid.org/0000-0001-8039-1424
Hamid Ullah https://orcid.org/0000-0001-7304-8863
Asif Mahmood https://orcid.org/0000-0003-1803-8384

References

[1] Moussa R, Abdiche A, Khenata R and Soyalp F 2021 First principles calculation of the structural, electronic, optical and elastic properties of the cubic AlxGa1-xSb ternary alloy *Opt. Mater.* **113** 110850
[2] Vs G K and Mahesha M G 2020 Characterization of spray deposited ternary ZnSxSe (1-x) thin films for solar cell buffers *Surf. Inter.* **20** 100509

[3] Kamlesh P K, Kumari S and Verma A S 2020 Effect of hybrid density functionals on half–Heusler LiZnX (X = N, P and As) semiconductors: potential materials for photovoltaic and thermoelectric applications *Phys. Scr.* **95** 095806
[4] Svechnikova T E, Shelimova L E, Konstantinov P P, Kretova M A and Avilov E S 2005 Thermoelectric Properties of Single Crystals for Solid Solutions (Bi2Te3)1-xy (Sb2Te3) x (Sb2Se3)y *Inorganic. Mater.* **41** 1186–93
[5] Tan G, Zhao L D and Kanatzidis M G 2016 Rationally designing high-performance bulk thermoelectric materials *Chem. Rev.* **116** 12123–49
[6] Pejova B, Grozdanov I and Tanuševski A 2004 Optical and thermal band gap energy of chemically deposited bismuth (III) selenide thin films *Mater. Chem. Phys.* **83** 245–9
[7] Augustine S, Ampili S, Kang J K and Mathai E 2005 Structural, electrical and optical properties of Bi_2Se_3 and $Bi_2Se_{(3-x)}$ Tex thin films *Mater. Res. Bull.* **40** 1314–25
[8] Gorai P, Goyal A, Toberer E S and Stevanović V 2019 A simple chemical guide for finding novel n-type dopableZintl pnictide thermoelectric materials *J. Mater. Chem. A* **7** 19385–95
[9] Jappor H R, Obeid M M, Vu T V, Hoat D M, Bui H D, Hieu N N and Khenata R 2019 Engineering the optical and electronic properties of Janus monolayer Ga_2SSe by biaxial strain *Superlattices Microstruct.* **130** 545–53
[10] Zhong Q, Dai Z, Liu J, Zhao Y and Meng S 2019 *RSC Adv.* **9** 25471
[11] Naseri M and Hoat D M 2019 First principles investigation on elastic, optoelectronic and thermoelectric properties of KYX (X = Ge, Sn and Pb) half-heusler compounds *J. Mol. Graphics Modell.* **92** 249–55
[12] Ma Z, Yi Z, Sun J and Wu K 2012 Electronic and photocatalytic properties of Ag_3PC_4VI (C = O, S, Se): a systemic hybrid DFT study *J. Phys. Chem. C* **116** 25074–80
[13] Wei J and Wang G 2018 Thermoelectric and optical properties of half-Heusler compound TaCoSn: a first-principle study *J. Alloys Compd.* **757** 118–23
[14] Bell L E 2008 Cooling, heating, generating power, and recovering waste heat with thermoelectric systems *Science* **321** 1457–61
[15] Vineis C J, Shakouri A, Majumdar A and Kanatzidis M G 2010 Nanostructured thermo-electrics: big efficiency gains from small features *Adv. Mater.* **22** 3970–80
[16] Zhao L D, Dravid V P and Kanatzidis M G 2014 The Panoscopic Approach to High Performance Thermoelectrics *Energy Environ. Sci.* **7** 251
[17] Heremans J P, Dresselhaus M S, Bell L E and Morelli D T 2013 When thermoelectrics reached the nanoscale *Nat. Nanotech.* **8** 471–3
[18] Zhao L D, Lo S H, Zhang Y, Sun H, Tan G, Uher C and Kanatzidis M G 2014 Ultralow thermal conductivity and high thermoelectric figure of merit in SnSe crystals *Nature* **508** 373–7
[19] Wei P C, Yang C C, Chen J L, Sankar R, Chen C L, Hsu C H and Chen Y Y 2015 Enhancement of thermoelectric figure of merit in β-Zn_4Sb_3 by indium doping control *Appl. Phys. Lett.* **107** 123902
[20] Wu M and Zeng X C 2016 Intrinsic ferroelasticity and/or multiferroicity in two-dimensional phosphorene and phosphorene analogues *Nano Lett.* **16** 3236–41
[21] Kirkham M J, dos Santos A M, Rawn C J, Lara-Curzio E, Sharp J W and Thompson A J 2012 *Ab initio* determination of crystal structures of the thermoelectric material MgAgSb *Phys. Rev. B* **85** 144120
[22] Mak K F, Lee C, Hone J, Shan J and Heinz T F 2010 Atomically thin MoS_2: a new direct-gap semiconductor *Phys. Rev. Lett.* **105** 136805
[23] Ueda O, Fujii T, Nakada Y, Yamada H and Umebu I 1989 TEM investigation of modulated structures and ordered structures in InAlAs crystals grown on (001) InP substrates by molecular beam epitaxy *J. Crystal Growth* **95** 38–42
[24] Jen H R, Jou M J, Cherng Y T and Stringfellow G B 1987 The kinetic aspects of ordering in $GaAs_{1-x}Sb_x$ grown by organometallic vapor phase epitaxy *J. Crystal Growth* **85** 175–81
[25] Gomyo A, Suzuki T, Iijima S, Hotta H, Fujii H, Kawata S, Kobayashi K, Ueno Y and Hino I 1988 Nonexistence of long-range order in $Ga_{0.5}In_{0.5}P$ epitaxial layers grown on (111) B and (110) GaAs substrates *Jpn. J. Appl. Phys.* **27** L2370
[26] Kuan T S, Kuech T F, Wang W I and Wilkie E L 1985 Long-range order in $Al_xGa_{1-x}As$ *Phys. Rev. Lett.* **54** 201
[27] Lefebvre I, Szymanski M A, Olivier-Fourcade J and Jumas J C 1998 Electronic structure of tin monochalcogenides from SnO to SnTe *Phys. Rev. B* **58** 1896
[28] Laref S, Meçabih S, Abbar B, Bouhafs B and Laref A 2007 First-principle calculations of electronic and positronic properties of $AlGaAs_2$ *Physica B* **396** 169–76
[29] Hou H J, Kong F J, Yang J W, Xie L H and Yang S X 2014 First-principles study of the structural, optical and thermal properties of $AgGaSe_2$ *Phys. Scr.* **89** 065703
[30] Hai-Jun H, Shi-Fu Z, Bei-Jun Z, You Y and Lin-Hua X 2010 First-principles calculations of the elastic, electronic and optical properties of $AgGaS_2$ *Phys. Scr.* **82** 055601
[31] Brik M G 2009 First-principles study of the electronic and optical properties of $CuXS_2$ (X = Al, Ga, In) and $AgGaS_2$ ternary compounds *J. Phys. Condens. Matter* **21** 485502
[32] Ma C G and Brik M G 2015 First principles studies of the structural, electronic and optical properties of $LiInSe_2$ and $LiInTe_2$ chalcopyrite crystals *Solid State Commun.* **203** 69–74
[33] Benmakhlouf A, Bentabet A, Bouhemadou A, Maabed S, Khenata R and Bin-Omran S 2015 Structural, elastic, electronic and optical properties of $KAlQ_2$ (Q = Se, Te): A DFT study *Solid State Sci.* **48** 72–81
[34] He L, Meng J, Feng J, Zhang Z, Liu X and Zhang H 2019 Insight into the characteristics of 4f-related electronic transitions for rare-earth-doped KLuS2 luminescent materials through first-principles calculation *J. Phys. Chem. C* **124** 932–8
[35] Blaha P, Schwarz K, Madsen G K, Kvasnicka D and Luitz J 2001 Wien2k *An Augmented Plane Wave + Local Orbitals Program For Calculating Crystal Properties* **60** https://scholar.googleusercontent.com/scholar.bib?q=info:ytiD2_BG36cJ:scholar.google.com/&output=citation&scisdr=CgXmejPjEOf0udvrXkY:AAGBfm0AAAAAYSjuRkZ9a0WEa7F9Ky4QwcBld3_mXxCq&scisig=AAGBfm0AAAAAYSjuRmajjkzCbYcLlIj359h-WHw9rdsD&scisf=4&ct=citation&cd=-1&hl=en
[36] Perdew J P, Ruzsinszky A, Csonka G I, Vydrov O A, Scuseria G E, Constantin L A and Burke K 2008 Restoring the density-gradient expansion for exchange in solids and surfaces *Phys. Rev. Lett.* **100** 136406
[37] Tran F and Blaha P 2009 Accurate band gaps of semiconductors and insulators with a semilocal exchange-correlation potential *Phys. Rev. Lett.* **102** 226401
[38] Noor N A, Rashid M, Mustafa G M, Khan M I, Mahmood A and Ramay S M 2020 Study of pressure induced physical properties of $ZnZrO_3$ perovskite using density functional theory *Chem. Phys. Lett.* **753** 137601
[39] Noor N A, Anwar U and Mahmood A 2020 Investigation of the rare earth-based $LaYO_3$ (Y = Cr and Mn) perovskites by ab-initio approach *Chem. Phys. Lett.* **739** 137031
[40] Saeed Y, Amin B, Khalil H, Rehman F, Ali H, Khan M I and Shafiq M 2020 $Cs_2NaGaBr_6$: a new lead-free and direct band gap halide double perovskite *RSC Adv.* **10** 17444–51

[41] Saeed Y, Kachmar A and Carignano M A 2017 First-principles study of the transport properties in bulk and monolayer MX3 (M = Ti, Zr, Hf and X = S, Se) compounds *J. Phys. Chem. C* **121** 1399–403
[42] Bromley M W and Mitroy J 2003 Variational calculation of positron-atom scattering using configuration-interaction-type wave functions *Phys. Rev. A* **67** 062709
[43] Wisesa P, McGill K A and Mueller T 2016 Efficient generation of generalized Monkhorst-Pack grids through the use of informatics *Physical Review B* **93** 155109
[44] Vitos L 2001 Total-energy method based on the exact muffin-tin orbitals theory *Physical Review B* **64** 014107
[45] Madsen G K and Singh D J 2006 BoltzTraP. a code for calculating band-structure dependent quantities *Comput. Phys. Commun.* **175** 67–71
[46] Togo A and Tanaka I 2015 First principles phonon calculations in materials science *Scr. Materialia* **108** 1–5
[47] Yi W, Tang G, Chen X, Yang B and Liu X 2020 qvasp: a flexible toolkit for VASP users in materials simulations *Comp. Phys. Commun.* **257** 107535
[48] Murnaghan F D 1944 The compressibility of media under extreme pressures *Proc. National Acad. Sci.* **30** 244
[49] Jain A, Ong S P, Hautier G, Chen W, Richards W D, Dacek S and Persson K A 2013 Commentary: The Materials Project: A materials genome approach to accelerating materials innovation *APL Mater.* **1** 011002
[50] Yaqoob N, Murtaza G, Iqbal M W, Noor N A, Mahmood A, Ramay S M and Al-Garadi N Y 2020 Study of half metallic nature and transport properties of XMnSe2 (X = Ca, Sr and Ba) compounds via ab-initio calculations *J. Mater. Res. Tech.* **9** 10511–9
[51] Ziani N S, Seddik T, Bouhani-Benziane H, Betine K, Belfedal A and Sahnoun M 2019 First principles investigations of electronic and thermoelectric properties of BeSiPn2 (Pn=P, As) chalcopyrite compounds *Solid State Commun.* **302** 113731
[52] Nolan M, Grigoleit S, Sayle D C, Parker S C and Watson G W 2005 Density functional theory studies of the structure and electronic structure of pure and defective low index surfaces of ceria *Surface Sci.* **576** 217–29
[53] Chakrabarty S, Mandia A K, Muralidharan B, Lee S C and Bhattacharjee S 2019 Semi-classical electronic transport properties of ternary compound $AlGaAs_2$: role of different scattering mechanisms *J. Phys. Condensed Matt.* **32** 135704
[54] Aspnes D E, Kelso S M, Logan R A and Bhat R 1986 Optical properties of $Al_xGa_{1-x}As$ *J. Appl. Phys.* **60** 754–67
[55] Horsley S A R, Artoni M and La Rocca G C 2015 Spatial kramers–kronig relations and the reflection of waves *Nat. Photonics* **9** 436–9
[56] Penn D R 1962 Wave-number-dependent dielectric function of semiconductors *Phys. Rev.* **128** 2093
[57] McCrackin F L, Passaglia E, Stromberg R R and Steinberg H L 1963 Measurement of the thickness and refractive index of very thin films and the optical properties of surfaces by ellipsometry *J. Research of the National Bureau of Standards. Section A, Physics and chemistry* **67** 363
[58] Jiao Z Y, Ma S H and Yang J F 2011 A comparison of the electronic and optical properties of zinc-blende, rocksalt and wurtzite AlN: a DFT study *Solid State Sci.* **13** 331–6
[59] Chen J, Lin C, Peng G, Xu F, Luo M, Yang S and Ye N 2019 $BaGe_2Pn_2$ (Pn = P, As): Two congruent-melting non-chalcopyrite pnictides as mid-and far-infrared nonlinear optical materials exhibiting large second harmonic generation effects *Chem. Mater.* **31** 10170–7
[60] Aguilera I, Palacios P and Wahnón P 2008 Optical properties of chalcopyrite-type intermediate transition metal band materials from first principles *Thin Solid Films* **516** 7055–9
[61] Salehi H and Gordanian E 2016 *Ab initio* study of structural, electronic and optical properties of ternary chalcopyrite semiconductors *Mater. Sci. Semi. Pro.* **47** 51–6
[62] Mahmood Q, Alhossaiy M H, Rashid M S, Flemban T H, Althib H, Alshahrani T and Laref A 2021 First-principles study of lead-free double perovskites Rb2TeX6 (X = Cl, Br, and I) for solar cells and renewable energy *Mater. Sci. Eng. B* **266** 115064
[63] Zanib M, Noor N A, Iqbal M A, Mahmood I, Mahmood A, Ramay S M and Uzzaman T 2020 Density functional theory study of electronic, optical and transport properties of magnesium based MgY2Z4 (Z = S and Se) spinels *Current Appl. Phys.* **20** 1097–102
[64] Yasukawa M, Kono T, Ueda K, Yanagi H and Hosono H 2010 High-temperature thermoelectric properties of La-doped $BaSnO_3$ ceramics *Mater. Sci. Eng. B* **173** 29–32
[65] Li J, Yang J, Shi B, Zhai W, Zhang C, Yan Y and Liu P F 2020 Ternary multicomponent Ba/Mg/Si compounds with inherent bonding hierarchy and rattling Ba atoms toward low lattice thermal conductivity *Phys. Chem. Chem. Phys.* **22** 18556–61
[66] Gunatilleke W D, Hobbis D, Poddig H, Tinkess A, Beekman M, Wang H and Nolas G S 2020 *Structural, Electronic, and Thermal Properties of CdSnAs2 Inorganic chemistry* **59** 3079–84